Deformation, strength and tectonic evolution of basal ice in Taylor Glacier, Antarctica

Sean Fitzsimons[1], Denis Samyn[2], and Regi Lorrain[3]

[1]School of Geography, University of Otago, P.O. Box 56, Dunedin, New Zealand.

https://orcid.org/0000-0003-0513-7367

[2] Independent researcher, formerly at Laboratoire de Glaciologie, Faculté des Sciences, Université Libre de Bruxelles, Belgium.

[3] Retired, Laboratoire de Glaciologie, Faculté des sciences, Université Libre de Bruxelles, Belgium.

Corresponding author: Sean Fitzsimons (sean.fitzsimons@otago.ac.nz)

Key Points:

- Observations made in tunnels excavated in Taylor Glacier reveal a 4 m-thick basal ice sequence
- Sliding or highly localized deformation in thin zones occurs at structural interfaces within the basal ice
- About 60% of glacier surface velocity can be attributed to deformation within the 4.5 m thick sequence of basal ice

Abstract

Observation and measurements of ice structure and deformation made in tunnels excavated into the margin of Taylor Glacier reveal a complex, rapidly deforming basal ice sequence. Displacement measurements in the basal ice, which is at a temperature of -18°C, together with the occurrence of cavities and slickenslides, suggests that sliding occurs at structural discontinuities within the basal zone although we cannot rule out the possibility of rapid deformation in thin zones of high shear. Strain measurements show that the highest strain rates occur in ice with average debris concentrations of 26% followed by ice with debris concentrations of around 12%. The lowest strain rates occur in clean ice that has very low debris concentrations (<0.02%). Deformation within the basal ice sequence is dominated by simple shear but disrupted by folding which results in shortening of the debris-bearing ice followed by attenuation of the folds due to progressive simple shear which generates predominantly laminar basal ice structures. About 60% of glacier surface velocity can be attributed to deformation within the 4.5 m thick sequence of basal ice that was monitored for this study, and 15% of motion can be attributed to sliding. The combination of high debris concentrations and high strain rates in the debris-bearing ice means that material transported in the basal ice is exposed to a high rates of abrasion which produces heavily striated and facetted clasts typical of temperate glaciers even though the basal ice is at a temperature of -18°C.

1 Introduction

The most significant glacial processes occur at the beds of glaciers within a few metres of the contact between ice and the glacier substrate. Deformation of ice and debris close in this zone regulates the nature of motion at the bed, the rate of deformation experienced by ice and the deformation and entrainment of subglacial sediment (Clarke, 2005; Hubbard, 2006; Iverson, 2010). One of the products of glacier-substrate interactions is basal ice which can be defined as ice close to the bed of glaciers that has distinctive physical, chemical and mechanical properties (Hubbard & Sharp, 1989; Hubbard et al., 2009). These properties are imparted by interactions between glacier ice and the substrate. The processes that occur within basal ice and at glacier beds underpin the large-scale behaviour of glaciers and control the geological processes at the ice-substrate interface. These processes also determine the geological imprint of glaciation on the Earth's surface (Alley et al., 1997; Boulton, 2006; Iverson, 2010).

Debris and solutes within basal ice alter the rheology of materials close to the bed which has direct implications for glacier behaviour and glacial geological processes. For example, a cold-based glacier with easily deformable basal ice will have higher surface velocities and a thinner surface profile than a cold-based glacier without easily deformable ice (Pettit et al., 2014). Both experimental and field-based research on the behaviour of ice/debris mixtures suggests that we do not yet understand the constitutive properties of debris-ice mixtures (Moore, 2014; Thompson et al., 2020). There is a substantial body of experimental data that suggests the addition of solid debris increases ice strength (Goughnor & Andersland, 1968 Nickling & Bennett, 1984; Waller, 2001; Fitzsimons, 2006; Waller et al., 2012). However, field observations remain equivocal (Moore, 2014). Some studies have determined that ice containing debris is stronger than adjacent pure ice (Rabus and Echelmeyer,1997; Fitzsimons et al., 1999, 2000, 2008; Fitzsimons & Howarth, 2020; Fitzsimons et al., 2023) whereas others have concluded that ice containing debris is weakened relative to adjacent ice (Echelmeyer & Zhongxiang, 1987; Cohen, 2000). Using compressive strength tests on ice from Taylor Glacier Lawson (1996) showed that the addition of 10% debris by volume resulted in increases and decreases in ice

viscosity. Although some studies have concluded that the addition of debris has no impact on the strength of the ice (Cuffey et al., 2000; Jacka et al., 2003; Moore, 2014) the general view is that sediment in ice is expected to be stronger than adjacent ice and less susceptible to ductile deformation well below the freezing point (Moore, 2014; Warbritton et al., 2020). In an extensive review of the behaviour of frozen debris Moore (2014) concluded that ice-debris mixtures are more resistant to deformation at low temperatures than pure ice but that at temperatures closer to melting the growth of a interfacial water film can lead to profound weakening. Collectively this work has demonstrated that there are several key gaps in our understanding and the complexity of linkages between ice, debris, and glacier behaviour remains elusive.

Taylor Glacier is an outlet glacier that flows from Taylor Dome which is part of the East Antarctic Ice Sheet (Figure 1). The glacier terminates in the McMurdo Dry Valleys at the permanently ice-covered Lake Bonney where the ice margin is characterized by 18-20 m high cliffs. At the glacier terminus Robinson (1984) measured a mean ice surface temperature of −17°C and concluded that the glacier was at the pressure melting point some distance upstream of the terminus. Using an ice penetrating radar Hubbard et al. (2004) concluded that upstream of the glacier terminus the bed consisted of saturated sediment or ponded liquid. Later work has mapped widespread hypersaline groundwater that is connected to Blood Falls, a hypersaline water discharge at the glacier terminus (Foley et al., 2016; Mikucki et al., 2015; Badgely et al., 2017). Study of ice-crystal textures and gas content of the basal ice from Taylor Glacier show that significant shearing has occurred within this basal ice (Samyn et al., 2005a) and inferred that that variations in resistance to deformation occur at the cm to mm-scale within the basal ice. Pettit et al. (2014) used a two-layer flowband model to investigate glacier behaviour and concluded that the basal ice contributes 85-90% of glacier surface velocity and that the basal ice was likely 10-15 m-thick and 20-40 times softer that Holocene age glacier ice. These findings suggest that at least in some circumstances cold-based glaciers can be very sensitive to subglacial deformation processes.

Here we hypothesize that strain in the basal zone of Taylor Glacier is localized to thin bands of intense shear or sliding and that deformation of the basal ice is the major component of glacier surface velocity. We further hypothesize that despite the low temperature at the margin of this glacier localized shear and potentially sliding results in a structural evolution of the basal zone and that these processes impart a distinctive glacial geological signature. This paper describes the geomorphological setting and the methods used in the study (Section 2), and presents observations of the composition and deformation of the basal zone from a combination of field and laboratory analyses (Section 3). Interpretation of the data focuses on the patterns of ice deformation, the rheological controls of deformation in the basal zone of the glacier, and the geological imprint of these processes (Section 4).

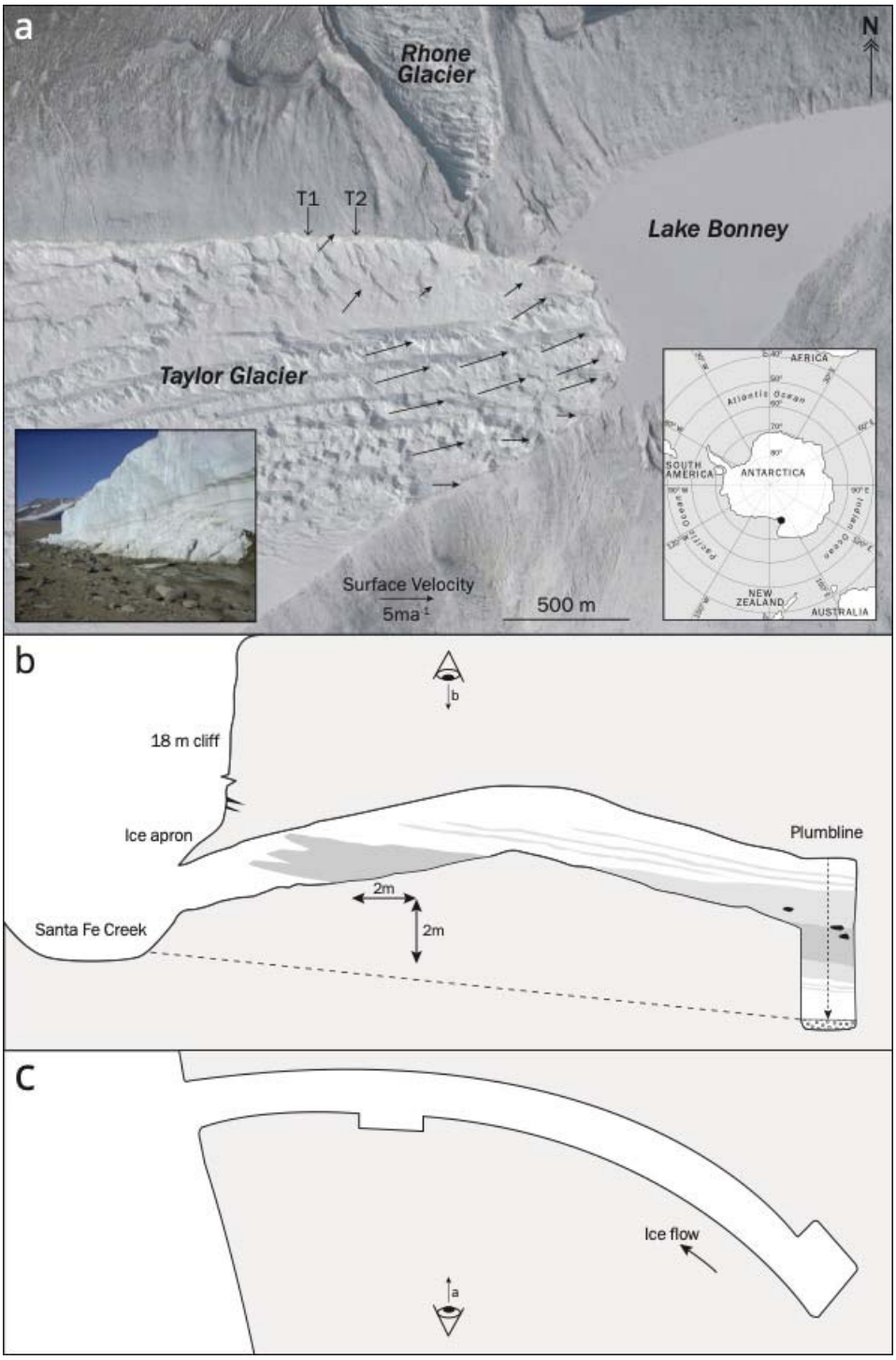

104

105 **Figure 1**. (a) Location map of Taylor Glacier showing the location of the tunnels (T1 and T2)
106 and the velocity distribution over the terminus area. Base image: Google Earth, CNES/Airbus,
107 image date: 22 November 2016. (b) and (c) Elevation and plan of the second tunnel excavated in
108 1999.

2 Data and methods

2.1 Excavation

In the austral summer of 1998-1999 a 20 m-long tunnel was excavated approximately 1.1 km upstream of the terminus at 77.71994°S 162.21939°E (T1 in Figure 1) using electric chainsaws with tungsten carbide cutters on the chain to make relief cuts in the ice, a demolition hammer to break up the ice and a sled to remove the ice from the tunnel. This tunnel was studied for a 2 week period but was destroyed by a combination of melting and flooding before it could be resurveyed the following summer. A second tunnel was excavated and instrumented in December 1999 approximately 200 m downstream of the first tunnel at 77.72068°S 162.22854°E (T2 in Figure 1). This tunnel was resurveyed in January 2000 and again in November 2000. The tunnelling process is documented in a series of short videos stored in Zenodo (Fitzsimons, 2023). The temperature of the ice measured along the tunnel was -18±1°C beyond 8 m of the tunnel entrance (Figure 2). The air temperature at the back of the tunnel remained around -15°C during excavation. Both tunnels were approximately 20 m-long and curved to avoid direct sunlight getting into the tunnels. The walls were oriented parallel to ice flow at the end of each tunnel. A 4 m-deep shaft was cut at the end of the second tunnel to expose the debris-bearing basal ice (Figure 3). Most of the observations and data reported in this paper come from the second tunnel.

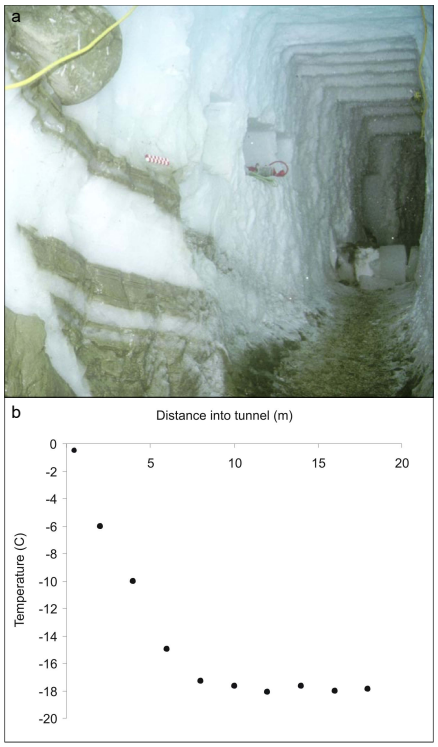

Figure 2. (a) Entrance to the second tunnel after excavation showing basal debris layers rising toward the ice edge. The abrupt termination in the debris layers is the contact between the basal ice and the marginal ice apron. A 500 mm-diameter boulder rests on the top of the basal debris layer in the upper left corner of the photograph. (b) Temperature measured using thermocouples placed in holes drilled 200 mm into the tunnel wall from the entrance to the end of the tunnel.

133 2.2 Debris characteristics

134 The particle size distribution of sediments was determined by treating subsamples with 5
135 ml of 30% H_2O_2 to digest organic matter and rinsed in de-ionised water. Biogenic silica was
136 removed using 10 ml of 1 M NaOH and rinsed with de-ionised water. The samples were then
137 treated with 5 ml of 5% sodium hexametaphosphate solution and shaken gently for two hours to
138 deflocculate clay-sized particles. The treated samples were analysed using a Malvern Mastersizer
139 2000 laser particle size analyser or sieved if the samples contained particles >2 mm in diameter.

140 Debris concentration measurements were made by displacing the samples in water to
141 determine volume, then the sample was melted, the water evaporated and the remaining sediment
142 weighed. Debris concentration are expressed as percentages of volume calculated using a particle
143 density of 2700 $kg.m^{-3}$.

144 Three representative samples of 30 particles > 40 mm in diameter were retrieved by
145 melting blocks of the massive ice facies (section 4.1). These particles were examined for
146 striations and their shape was classified using Powers roundness classes (Powers, 1953).

147 2.3 Ice motion measurements

148 Measurements of ice movement were obtained using plumblines and engineers dial
149 gauges that were rock-bolted to boulders in the basal ice. The dial gauges used were Mitutoyo
150 series 2 gauges that have a precision of ±0.02 mm and an accuracy of ±20 μm. The plumblines
151 consisted of nylon lines attached to a peg drilled and frozen into the top of the tunnel wall
152 (Figure 3a). The line was held taut with a plumb bob which was mounted above a brass target
153 drilled and frozen into the tunnel floor. Displacements were measured from the plumbline and
154 wooden markers drilled and frozen into the ice at 100 mm intervals using a digital caliper for
155 displacements up to 200 mm and a steel tape for displacements >200 mm. The plumblines were
156 resurveyed at intervals of 27, 42 and 403 days between December 1999 and November 2000.
157 Although the motion of brass target on the floor were measured and appeared to be stationary,
158 we cannot entirely discount the possibility that it is moving.

159 2.4 Strain measurements

160 Ice strain was measured using strain arrays that consisted of square arrays of stainless
161 coach screws that were drilled and frozen into the tunnels walls parallel to the ice flow (Figure
162 3b). Each stainless steel coach screw had a cone milled into its head in order to accurately
163 position a digital caliper that had locating cones fixed to the jaws. Measurements were made
164 using a Mitutoyo digital caliper with a precision of 0.001 mm. The caliper was calibrated by
165 repeat measurements of cones milled into a block of stainless steel. Repeated measurements of
166 the calibration block resulted in an operator error of ± 0.0096 mm and an accuracy of ±0.02
167 (n=60). All the strain rates reported in this paper are based on measurements between 42 and 403
168 days. During this time, some bulging of the tunnel walls occurred, which could introduce errors
169 related to differences in closure rates in different basal ice facies. This problem is addressed in
170 section 2.7 of this paper. Bulging the the tunnel walls were monitored by surveying the shape of
171 the tunnel over time

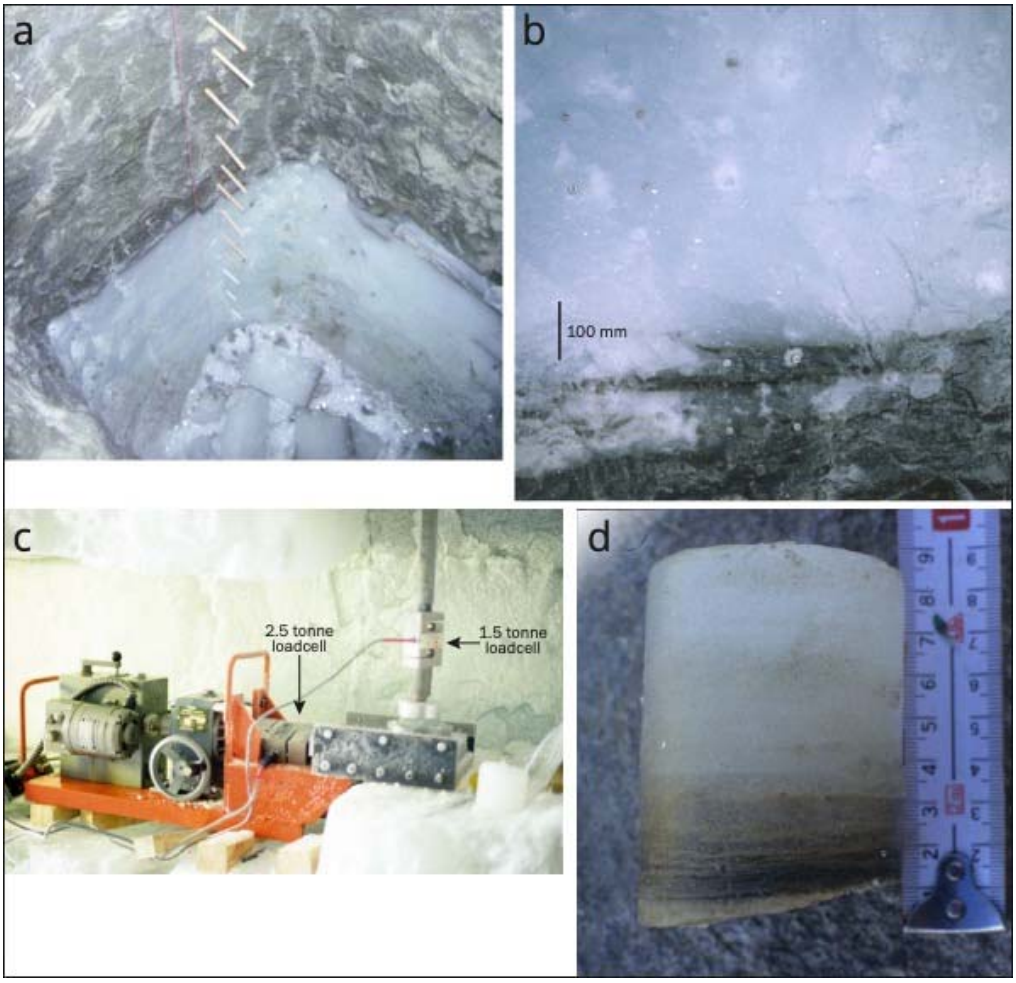

Figure 3. Monitoring ice deformation. (a) Plumbline and wooden pegs in the shaft excavated at the end of the tunnel. (b) Strain arrays of four stainless steel coach screws in the upper left and lower centre, located at the interface between debris bearing and clean ice. (c) Direct shear device used for *in situ* strength tests. At left is a Wykeham Farrance direct shear machine with a 2.5 tonne load cell between the stepper motor and the moving stainless steel plate. The vertical load is applied by a truck pneumatic shock absorber (out of view on the top of the vertical pole) separated from the top of the sample with a 1.5 tonne load cell. (d) Stratified debris-bearing ice sample tested in the direct shear device.

Strain rates were calculated from the corners of triangles defined from the strain arrays using a numerical calculation of a Mohr circle based on the method of Ramsay (1967) and used in glaciology by Hambrey and Müller (1978) and Hambrey et al. (1980). We have followed the convention for principal strain rates that $\dot{\boldsymbol{\varepsilon}}_{\mathbf{1}}$ and $\dot{\boldsymbol{\varepsilon}}_{\mathbf{3}}$ are horizontal, that $\dot{\boldsymbol{\varepsilon}}_{\mathbf{1}} \geq \dot{\boldsymbol{\varepsilon}}_{\mathbf{3}}$, that extension is positive, and that $\dot{\boldsymbol{\varepsilon}}_{\mathbf{3}}$ is always vertical (Sharp et al., 1988). Shear strain rate was calculated as: $\dot{\boldsymbol{\gamma}} = \frac{\dot{\varepsilon}_1 - \dot{\varepsilon}_2}{2}$. The analytical techniques and errors associated with the strain calculations derived from field measurements made in tunnels are described in Fitzsimons et al. (2008). If the walls of the tunnel did not bulge $\dot{\boldsymbol{\varepsilon}}_{\mathbf{3}}$would equal zero, which is not the case with any of the measurements. However, $\dot{\boldsymbol{\varepsilon}}_{\mathbf{3}}$ is an order of magnitude less than $\dot{\boldsymbol{\varepsilon}}_{\mathbf{1}}$ and both $\dot{\boldsymbol{\varepsilon}}_{\mathbf{1}}$ and $\dot{\boldsymbol{\gamma}}$ increase into the tunnel so

we conclude that tunnel closure has not introduced major errors into the calculation of strain rates. $\dot{\varepsilon}_2$

2.5 Ice sampling

Samples of basal ice were collected for chemical and structural analysis using a chainsaw in ice with relatively low debris concentrations and a 59 mm diameter diamond corer where the ice contained high debris concentrations or larger particles. Following collection, the frozen samples were returned to the laboratory where they were subsampled in a freezer using a band saw to produce samples of about 50 ml. After subsampling, the ice was melted at room temperature within 10 min. of being cut and immediately filtered with 0.45 μm cellulose nitrate filter paper. The laboratory procedure is described in Fitzsimons et al. (2008).

2.6 Direct shear tests

A series of direct shear tests were undertaken in the tunnel using a modified laboratory direct shear device (Figure 3c). The shear box was constructed on stainless steel plates that were drilled to accommodate a 59 mm diameter cylindrical sample (Figure 3d) and driven by a stepper motor through a load cell to move the upper plate (Figure 3c). The device was capable of displacing the sample by about 5 mm which is a strain of approximately 8%. Shear test samples were cut from the basal ice using a diamond corer driven by an electric drill. The experiments were conducted in the tunnel which had an air temperature of -15°C, with displacement rates of 0.85 $mm.h^{-1}$ and a normal load of 200 kPa. The normal load was applied by a pneumatic truck shock absorber attached to the tunnel roof and a load cell above the sample (Figure 3c). The tests were run for 3 to 4 hours to reach peak shear strength.

2.7 Limitations

Making ice deformation measurements in tunnels is problematic because any instruments introduced into the glacier bed run the risk of changing the boundary conditions that they are designed to measure. This is particularly the case with tunnels cut into glacier margins because the ice will tend to creep into the tunnel. In this study we have attempted to mitigate the effects of creep of the tunnel walls from the strain measurements by a combination of orienting the planes in which measurements were made parallel to ice flow, and by simultaneously recording deformation of the tunnel walls. Although the presence of the tunnel has changed the strain behaviour of the ice, the measurements we made are consistent with the results of the direct shear tests which leads us to conclude that the measurements we have made capture the relative differences between the three main ice facies and sub-facies that were present at Taylor Glacier described in section 4, below.

3 Results

3.1 Physical characteristics of the basal ice

Three distinctly different facies can be identified in the basal zone; clean englacial ice, stratified ice that consists of two subfacies, and a coarse pebble-cobble gravel at the bottom of the excavation (Table 1). The stratified facies consists of two subfacies: a laminated subfacies

228 composed of alternating laminae of debris-bearing and; clear clean ice layers 1 to 5mm thick and
229 a massive subfacies that has an unstructured appearance.

230

231 **Table 1**

232 Basal Ice Facies Characteristics
233

Facies	Subfacies	Debris concentration [% vol.]		Physical characteristics
		Mean	s.d.	
Englacial		0.19	0.4	Bubbly white ice with very low debris concentrations.
Stratified	Laminated	21.0	15.6	Thin laminae of debris bearing ice alternating with laminae of clean, clear, bubble-free ice. Both laminae are <5 mm wide
	Massive	33.2	2.6	Debris bearing ice with massive (structureless) appearance. Wide range of particle sizes from boulders 1.5 m in diameter to silt -sized particles.
Gravel		65	-	Cobble and pebble gravel at the base of the excavation, ice confined to pore spaces.

234

235 The clean englacial ice consists white bubbly ice with very low debris concentrations that
236 average 0.19% (Figure 3b, Table 1). The debris consists of dispersed silt to sand-sized particles
237 and most of the stretched bubbles have axial ratios between 1:3 and 1:5. The laminated subfacies
238 consists of finely laminated debris-rich ice and clean, clear ice layers (Figure 4a and 4b).
239 Individual laminae range from 5 mm to less than 1 mm-thick and the debris ranges from
240 abundant silt-sized particles up to boulder-sized particles held in the ice (Figure 2). The massive
241 subfacies consists of densely-packed debris in a matrix of clear, clean ice. Although this ice has
242 the appearance of being massive sections cut from the ice reveal the presence of abundant clear,
243 clean ice lenses and laminae (Figure 4c and d). Average debris concentrations in this subfacies
244 are 33.2 % vol. The very low standard deviation (2.6) reflects remarkably uniform debris
245 concentrations in the central part of this subfacies (Table 1).

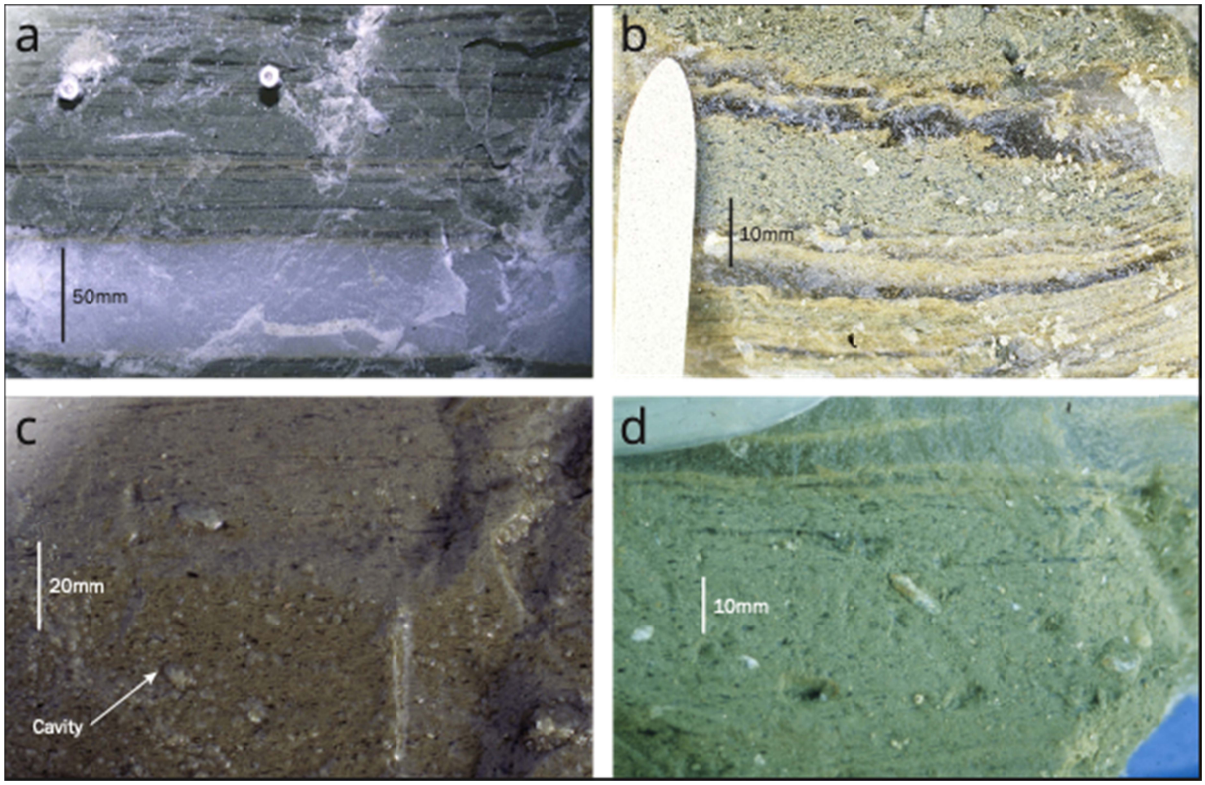

Figure 4. Basal ice facies exposed in the tunnel walls. (a) Laminated subfacies interbedded with the clean facies. The two bolts shown in the upper part of the photograph are part of a strain array. (b) Laminated subfacies with folded and sheared layers of clean bubble-free ice. (c) Massive facies with clear ice lenses and small pebble with stoss and lee-side cavities. (d) Massive facies with small pebbles. Ice flow is from right to left in all photographs.

The bottom of the shaft consisted of a 300 mm-thick coarse cobble-pebble gravel that stopped the excavation. Attempts to drill through the gravel with an ice auger equipped with tungsten carbide cutters and an attempt to map the geometry of the unit with a ground penetrating radar were unsuccessful.

Solute concentrations are highly variable in the basal ice (Table 2). The englacial ice is characterised by low concentrations in Cl^- and the major cations, and the values have a low standard deviation. The laminated subfacies is characterised by moderate concentrations of Cl^- and the major cations with a relatively high standard deviation likely reflecting two subpopulations of the clean clear laminae and the debris-bearing laminae. The highest solute concentrations were found in the massive subfacies where Cl^- is an order of magnitude greater than the laminated subfacies and the major cations are all at least three times the values of the laminate subfacies, with the exception of Na^+ which is lower than the value for the laminated subfacies (Table 2). The high standard deviation of of the partial TDS measure shows that there is very high variability in the values in both stratified subfacies.

Table 2

Average Solute Concentrations for the Ice Facies [a]

Facies (number of samples)	Cl^-	Na^+	Ca^{2+}	K^+	Mg^{2+}	TDS[a]	s.d.
Englacial (16)	0.28	0.41	0.55	0.03	0.04	1.31	0.68
Stratified laminated subfacies (21)	82.00	39.43	123.84	5.93	4.10	280.20	236.05
Stratified, massive subfacies (5)	1084.07	22.30	394.30	59.55	21.30	1581.53	1716.41

[a] Values in parts per thousand

[b] Partial measure of Total Dissolved Solids

3.2 Sedimentology and structure

Both the laminated and massive subfacies contain dolerite, gneiss and granite boulders up to 600 mm in diameter (Figure 2). A selection of pebble to cobble-sized particles were recovered from the ice by allowing the ice matrix of samples to sublimate. These particles were frequently faceted and exhibited striae in cross cutting patterns with fine rock debris preserved adjacent to the striae (Figure 5a, b). Although not as well developed or abundant as striae on dolerite particles, gneiss and granite clasts also exhibited striae in cross-cutting directions, primarily on protuberances on the particles (Figure 5b). The cross-cutting striae suggests substantial rotation of the particles within the basal ice during abrasion. A few striated ventifacts were recovered from the laminated subfacies.

Particle size distributions of the sediment fractions less that 3.5 ϕ (11 mm) from the massive and laminated subfaces show that all the samples were very poorly sorted and characterized by multi modal distributions (Figure 5c, d and e). The largest peak in the distributions occurs between 3.5 and 4.0 phi (0.088 to 0.062 mm), which encompasses fine sand and coarse silt particles. A persistent secondary peak occurs at 2 phi (4 mm), which is composed of fine gravel particles. The modal particle shape is subangular but there are large numbers of subrounded and angular particles (Figure 5g and h).

Although the laminated and massive subfacies are dominated by planar structures (Figure 6), numerous ductile deformation structures were observed, particularly in the laminated subfacies. Figure 6a shows a thin section of a layer of the laminated subfacies between two layers of englacial ice and there is a strong contrast in the diameter of ice crystals in the two facies. Two 10-15 mm diameter pebbles show that the ice layers are warped over the particles and that there are dark shadow zones on the stoss and lee sides of the pebbles, some of which are air-filled cavities.

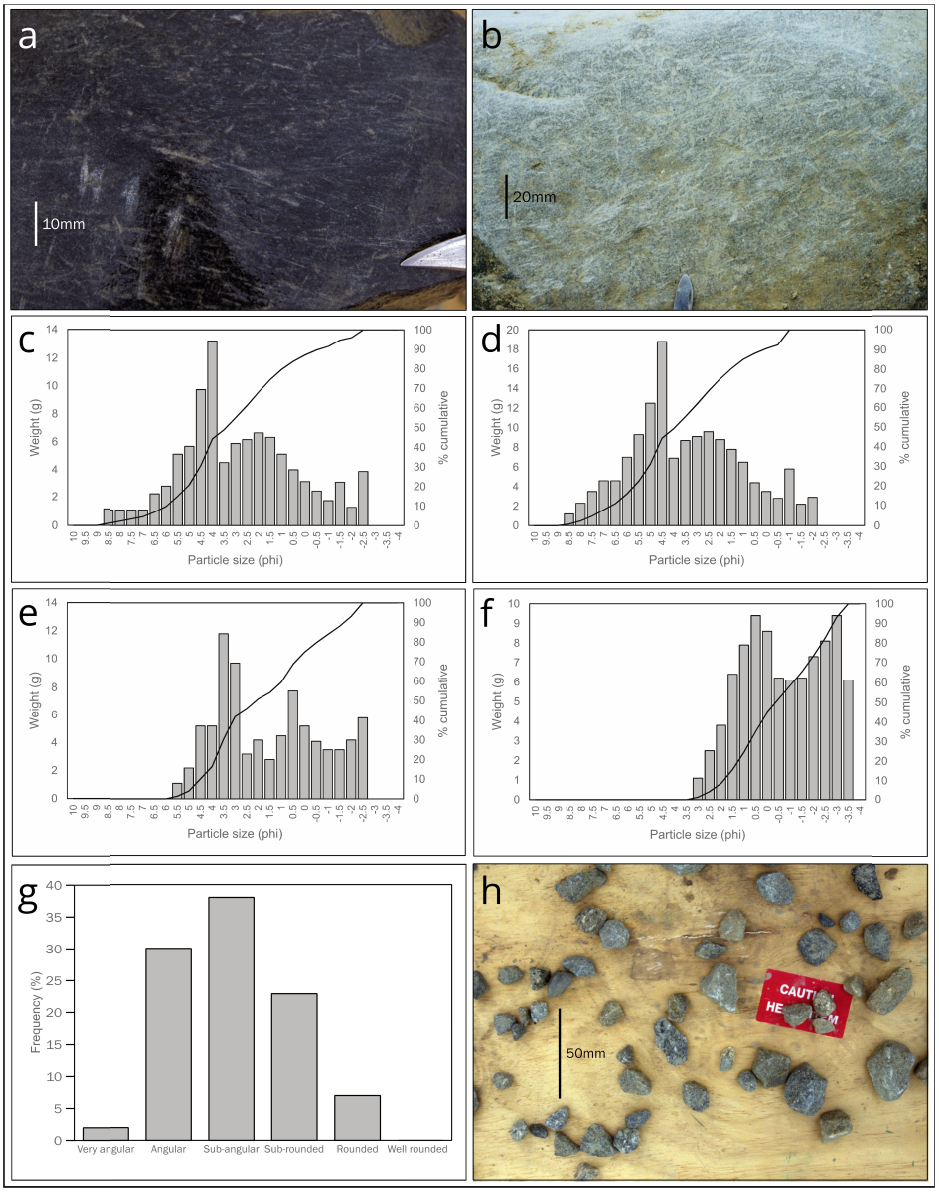

Figure 5. Characteristics of debris in the basal ice and adjacent surficial sediments. (a) Randomly oriented striae on a polished dolerite clast (b) Randomly oriented striae on a gneiss clast. The striae appear "fresh" judged from the presence of powdered rock debris adjacent to striations. Both cobbles are from the top of the main debris band 3-3.5 m above the datum. (c) Particle size distribution from the center of the massive subfacies debris band 2.8 m above the shaft datum. (d) Particle size distribution from the top of the main debris band 3.4 m above the datum (e) Particle size distribution from the laminated subfacies facies 3.6 m above the datum. (f) Particle size distribution from the stream channel adjacent to the ice margin. (g) Roundness of pebbles from the main debris band classified using Powers roundness classes (Powers, 1953). (h) Predominantly subangular pebble-sized particles retrieved from melting 10kg of ice from the massive subfacies 3 m above the datum.

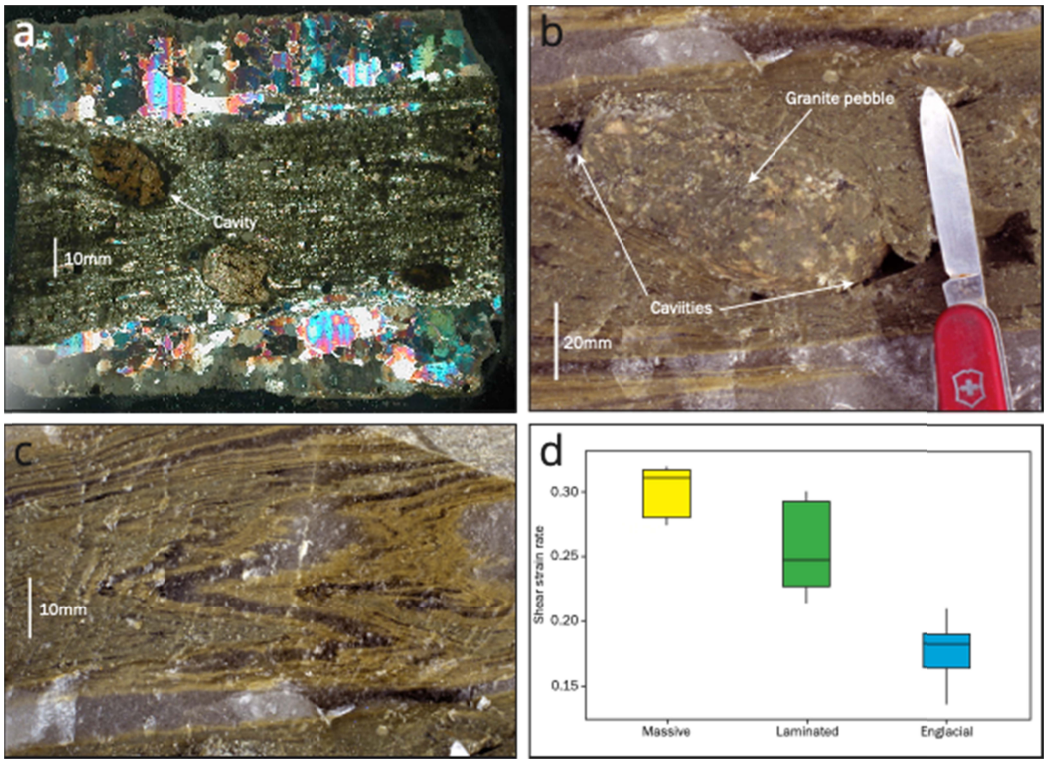

Figure 6. Deformation structures in the laminated subfacies. (a) Thin section under polarized light showing clean ice ice above and below a layer of the laminated subfacies. Ice crystals in the debris-bearing ice a less that 1 mm in diameter and the clean ice has crystals 5-10 mm in diameter. (b) Prolate-shaped particle in the debris-bearing ice with characteristic stoss and lee-side air filled cavities. (c) A tight polyharmonic recumbent fold with multiple shear bands extending into the overlying ice. (d) Box and whisker plot of the shear strain rate showing median, upper quartile ranges and the maximum and minimum values. The ice flow is from right to left in all photographs.

322 3.3 Strength of the basal ice

323 The direct shear tests show that the clean ice has the highest shear strength, followed by
324 the laminated subfacies and the massive subfacies (Table 3). The massive subfacies has half the
325 average shear strength of the englacial samples. The average peak shear strength of the samples
326 from the different facies are significantly different from each other (t-tests with p values between
327 0.000 and 0.008) and the tests have low standard deviations. The shear strain rate calculated from
328 the strain arrays shows that the materials with the highest strength, the englacial facies, have the
329 lowest strain rates and the lowest strength materials, the massive subfacies, have the highest
330 shear strain rates (Table 3). A few triaxial tests using samples cut so that the layers are 45° to the
331 long axis of the samples were undertaken in laboratory conditions. Although fewer in number,
332 the results of these test are in the same order as the direct shear tests conducted in the field
333 shown in Table 3. While some of these tests of resulted in barrel-shaped failures of the samples
334 many failed along ice layers within the laminated facies (Fig. 7).

335

336

337 **Figure 7.** Result of a triaxial test of a sample of the laminated subfacies showing failure
338 localized to an ice-rich layer in the laminated subfacies. This test was undertaken with the
339 sample in an air-filled pressure vessel maintained at 200kPa and -18°C for the duration of the 12
340 hr test.

341

342

343 **Table 3**

344 *Peak Shear Strength Values for Ice from the Basal Zone of Taylor Glacier*

345

Facies	Number of samples	Shear strength (MPa)[a]		Shear strain[b]
		Mean	s.d.	
Englacial	3	1.21	0.01	0.177
Laminated subfacies	5	0.91	0.11	0.257
Massive subfacies	4	0.64	0.01	0.301

346 [a] Mean peak shear strength from direct shear tests from direct shear tests done in the tunnel and
347 their standard deviations.

348 [b] Shear strain rate $\dot{\boldsymbol{\gamma}} = \frac{\dot{\varepsilon}_1 - \dot{\varepsilon}_2}{2}$, see section 2.4.

349 3.4 Ice motion and strain

350 3.4.1 Velocity of ice in the tunnel

351 A plumbline was located on the right wall in the shaft excavated at the end of the tunnel
352 (Figure 1) which spanned the 4.5 m section of the basal zone (Figure 8). Prominent offsets occur
353 in the displacement profile at 1.7 and 2. m above the measurement datum. The offset 1.7 m
354 above the datum is 74 mm.a^{-1} and the one located at 2.7 m is 130 mm.a^{-1}. Both the offsets occur
355 between pegs that were 100 mm apart at the boundaries the laminated and massive subfacies.
356 Displacements at the 1.7 m interface were also measured directly using engineers dial gauges
357 rock-bolted onto cobbles and boulders embedded massive subfacies but protruding into the
358 laminated subfacies. At the four locations measurements made over a period 4 to 31 days the
359 displacements ranged between 46 and to 167 mm.a^{-1}.
360
361

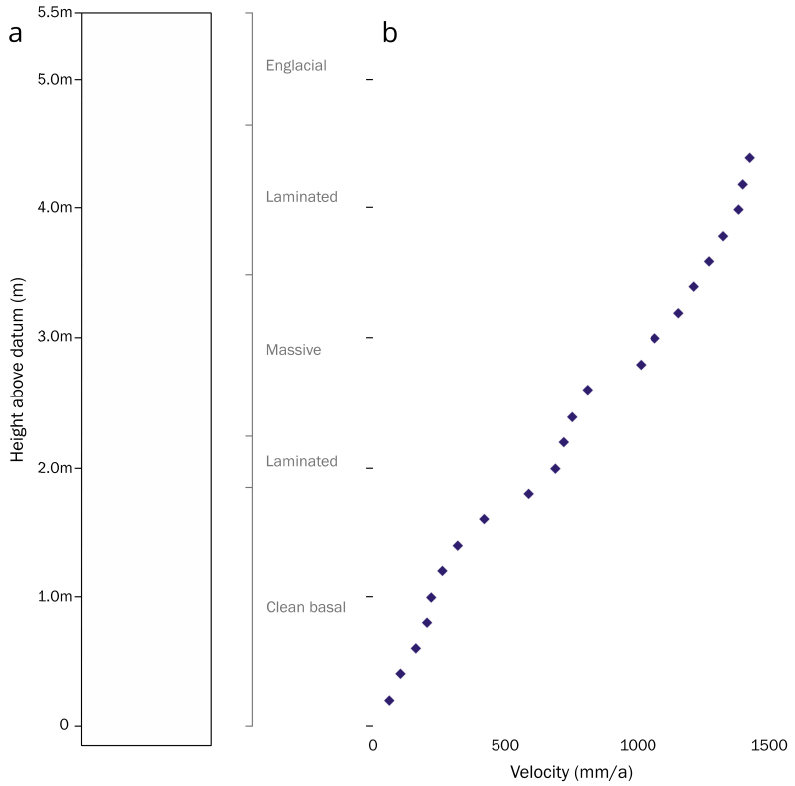

Figure 8. (a) Stratigraphic log of the shaft excavated at the end of the tunnel, showing clean glacier ice underlain by stratified ice consisting of laminated and massive subfacies. Granite boulders in the ice have lee and stoss-side air filled cavities shown as black zones. (b) Velocity measured with a plumbline surveyed episodically up to 403 days after installation. The two steps in the profile at 1.7 and 2.7 m above the datum occur at the interfaces between the massive and laminated subfacies facies.

3.4.2 Velocity of ice at the glacier surface

Optically surveyed velocity measurements between 2.1 $m.a^{-1}$ close to the ice margin to 5.5 $m.a^{-1}$ in the glacier center line over 376 and 769 days (Figure 1). The surface velocity close to the tunnel was 2.1 $m.a^{-1}$, which is within the error of a 2.5 $m.a^{-1}$, velocity determined by optical surveying of pegs placed in the cliff (B. Hubbard pers. comm. 2007). These velocity measurements are very similar to the magnitude and pattern of surface velocities determined by GPS surveying of stakes on the glacier surface (Pettit et al., 2014).

3.4.3 Strain of ice in the basal ice shaft

The highest shear strain rates are in the massive subfacies followed by the laminated subfacies and the englacial ice (Figure 6d). These differences align with observations made of tunnel closure and deformation of boreholes and strain markers cut into the tunnel walls. After 403 days the greatest deformation of the tunnel occurred in the shaft excavated at the end of the tunnel where the rectangular cross section of the tunnel was observed to deform into a keyhole

384 shape (Figure 9a). Cylindrical holes cut in the tunnel walls with a diamond corer deformed
385 rapidly in the laminated subfacies during the experiment (Figure 9b). Within 4 days the holes
386 deformed into ellipses with axial ratios between 1.38 and 1.53, whereas corresponding holes in
387 the low debris concentration laminated subfacies had average axial ratios of 1.2. There was no
388 detectable deformation of the holes in clean ice. Closure occurred fastest at the interface between
389 the laminated subfacies above and below the massive subfacies layer (Figure 9c). Bulging also
390 occurred in the back wall of the tunnel which was oriented transverse to ice flow (Figure 1). Here
391 the maximum rates of deformation occurred in the laminated subfacies and the bulging
392 resembled the shape of a plug (Figure 9d).
393

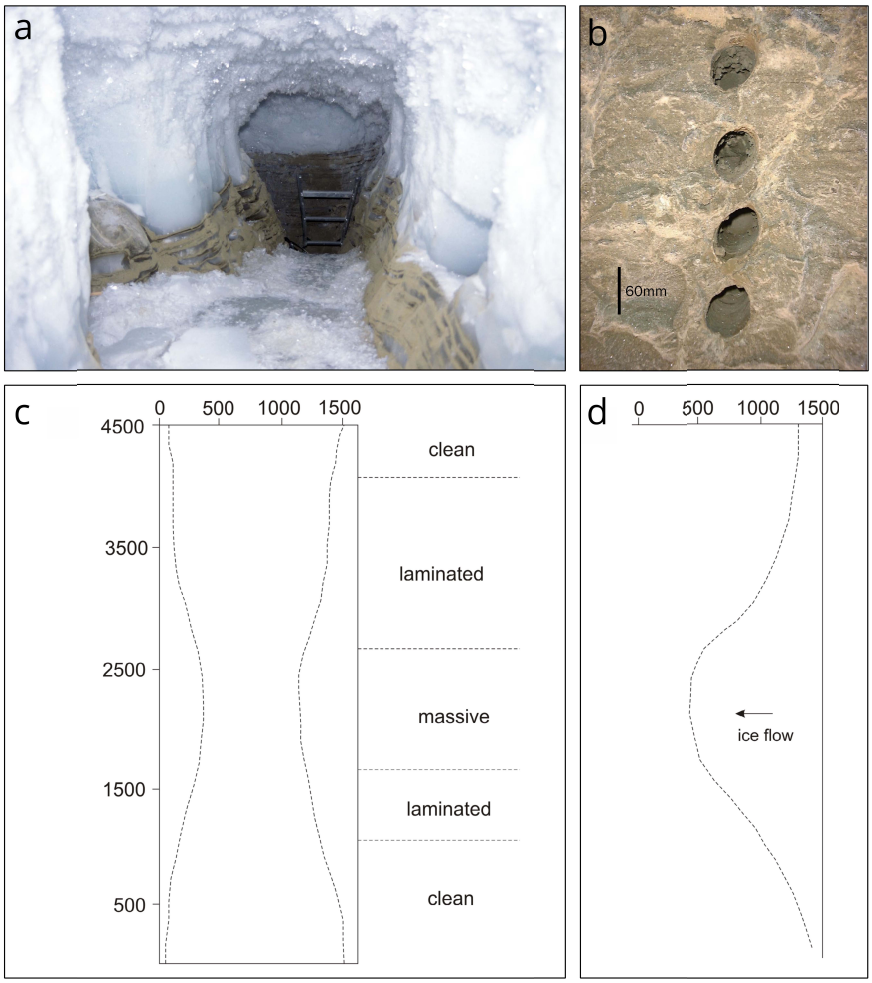

394

395 **Figure 9**. Evidence of the differential and localized deformation in the tunnel. (a) Photograph of
396 the end of the tunnel 403 days after excavation. The walls of the shaft were originally planar and
397 vertical. Most of the closure has occurred at the interface between the laminated and massive
398 subfacies in the lower part of the photograph. The end of the ladder is 600 mm wide. (b) Closure
399 of 59 mm diameter core holes in the massive subfacies 4 days after the samples were cored. (c)
400 Closure of the cross section of the shaft excavated at the end of the tunnel 403 days after
401 excavation. (d) Bulging of the rear wall of the tunnel surveyed 403 days after excavation.

4 Discussion

4.1 Motion in basal ice layer

The measurements made in the tunnel show that deformation is dominated by progressive simple shear within the debris bearing ice with strong differences in the rate of deformation in different ice facies. The highest rates of strain occur in the massive subfacies followed by the laminated subfacies and the englacial facies, a pattern that is the same order as the direct shear tests. Two exceptions to the pattern of progressive simple shear are the presence of offsets in the plumbline profile which maybe thin shear zone or sliding interfaces and the presence of polyharmonic recumbent folds which point to flow perturbations within the basal ice.

The offsets in the velocity profile recorded at 1.7 and 2.7 m above the datum occur at interfaces between the massive and laminated subfacies (Figure 8). Measurements of displacements on boulders at the upper interface, together with the development of air-filled cavities and slickenslides suggest there may be sliding at these interfaces. However, the spacing of the measurement pegs used in the plumbline (100 mm) preclude a definitive interpretation. The offsets could be produced by sliding or by narrow zones of higher rates of shear. Shear localization is also a feature of some triaxial tests (Figure 7). The possibility of sliding is discussed in section 6.2.

The deformation structures observed around particles in the laminated subfacies (Figure 6a) suggest a sense of vorticity (Samyn et al., 2009), and the pebbles appear very similar to sigma grains observed in deformed geological materials (Passchier & Simpson, 1986). Tight, recumbent, polyharmonic folds are common, particularly at the interfaces between the laminated facies and the massive facies (Figure 6c). Short wavelength parasitic folds that occur at the axes of the large folds are sheared in the direction of flow (Figure 6c). Such recumbent polyharmonic folds typically form in shear zones where instabilities develop at the boundaries of adjacent layers with different viscosities (Ramsay & Huber, 1987). This interpretation is consistent with our observations of folding at the interfaces between the laminated subfacies and the englacial ice and within the laminated subfacies where clean clear ice is interbedded with debris-bearing ice (Figure 4). The recumbent geometry of the folds together with the presence of numerous parasitic folds that appear to be sheared at the fold hinges (Figure 6c) suggests a sinistral rotation of objects in the basal ice (i.e. anticlockwise) and progressively attenuation that results in the pervasive laminar structure of the basal zone. In the predominantly compressive flow regime that characterizes the glacier margin the formation of folds leads to shortening and thickening of the basal layer.

A further source of instability in the basal zone are perturbations associated with pebble to boulder-sized particles that occur throughout the basal ice. Since these particles rest in a deforming medium in which deformation increases from bottom to top, the particles bridge a velocity gradient which results in sinistral rotation. In shear zones rotation occurs at a rate that can be significantly lower than the instantaneous shear strain rate (Simpson and De Paor, 1993). The combination of rotation of the particles and ice flowing over their upper surfaces has led to the development of morphologies similar to sigma grains in other geological materials. These particles are characterized by coatings of fine particles, striae in multiple directions, and pressure shadows at the stoss and lee sides of the grains. In the case of particles >10 mm in diameter, air-

444 filled cavities have developed adjacent to the clasts. (Figure 6b). Cavities on the margins of
445 boulder-sized particles were characterized by grooved linear markings on the cavity roofs. These
446 features resemble slickenslides in deformed rocks where polished and striated surfaces result
447 from friction produced at fault surfaces. The slickenslides are a series of grooves which are
448 impressions of the asperities of the particles that the ice has flowed over. Some of these cavities
449 degassed when punctured, i.e. the gas was above atmospheric pressure. Such cavities have also
450 been in the base of Suess Glacier, a small cold-based alpine glacier located about 12 km east of
451 Taylor Glacier (Fitzsimons et al., 2000).

452 Thin sections of small clasts (<10 mm) from the laminated subfacies show that the
453 pressure shadows consist of clear ice, which may be the product of recrystallization (Samyn et
454 al., 2005a). Ribbons of fine, elongated ice crystals at the boundaries of debris-bearing and clear
455 laminae identified in microstructural analysis occur where with the relative motion between ice
456 and particles being achieved by slip across low-viscosity interfacial water films (Samyn et al.,
457 2008). In addition, at the interface between the debris-rich and the clean ice layers of the
458 laminated subfacies, the ice crystals show clear signs of dynamic recrystallization and
459 differential strain. These patterns are indicative of the high rates of distributed shear and
460 relatively low strength of the in the debris-bearing facies identified in section 3.3.

461 4.2 Is sliding at -18°C plausible?

462 The two offsets in the velocity profile amount to 204 $mm.a^{-1}$ (130 mm at 2.7 m and 74
463 mm at 1.7 m above datum, Figure 8), which corresponds to 14% of motion within the basal zone
464 and about 8% of glacier motion at the ice edge (using 2.5 $m.a^{-1}$ as the ice edge surface velocity).
465 Taken together with the short-term point measurements of displacement above boulders and the
466 presence of cavities and slickenslides, these observations suggest two possibilities: sliding or
467 rapid deformation in thin (<100 mm) zones.

There is both theoretical and field evidence for sliding at subfreezing temperatures. Gilpin (1979) argued for the existence of liquid-like layers between the ice and the substrate, which led Shreeve (1984) and Fowler (1986) to suggest that sliding is possible at subfreezing temperatures. Subsequently sliding at has been observed or inferred at temperatures ranging between -1 and -17°C in several glaciers (Echelmeyer & Zhongxiang, 1987; Cuffey et al., 1999; Fitzsimons et al., 2000). In Meserve Glacier a small alpine glacier in the Dry Valleys with a basal temperature of -17°C displacement measurements at the ice boundary layer over boulders led Cuffey et al. (1999) to conclude that ice was sliding over the boulders at velocities between 2 and 8 $mm.a^{-1}$, which was ten times greater than the local strain rate. The sliding was associated with lee cavities on boulders which carried slickenslides like the ones described in this study. Cuffey et al. attributed the sliding at these low temperatures to the presence of interfacial films. Our point measurements on boulders range from 46 to 167 $mm.a^{-1}$ and the two offsets in the vertical profile at the upper and lower boundaries of the massive subfacies are 130 and 74 $mm.a^{1}$ respectively. If these displacements are from sliding, as seems likely, the velocities are more than an order of magnitude greater than those observed at Merserve Glacier at the same temperature. An important difference between the two sites is that the suspended sediment and solute concentrations in the basal ice at Taylor Glacier are considerably higher than in Meserve Glacier (Holdsworth, 1974; Samyn et al., 2005b). The ice is around 20 m thick at both locations.

The theory of premelting describes the formation and existence of liquid at temperatures below the solid region in a bulk phase diagram (Wettlaufer, 1999) and provides a useful theoretical context for field observations of subfreezing sliding. Surface premelting refers to the process in which a liquid or a liquid-like film is present at the surface of a crystal in contact with its vapor phase below the bulk freezing point, or at the junctions of crystals of the same material (Wettlaufer, 1999). The thickness of liquid films is extremely sensitive to the concentrations of solutes (Wettlaufer, 1999), and potentially to the nature of debris entrained within the ice (Dash et al., 1995). In Taylor Glacier the average total dissolved solids in the laminated and massive subfacies are two and three orders of magnitude greater respectively than that of the englacial ice. It is likely that the solute values are conservative because our samples were 10 mm wide and 100 mm long and provide average values through multiple laminae.

The high sediment concentrations in the massive subfacies together with the large component of fine sand and silt may also be conducive to sliding because finer-grained sediments are associated with depressed freezing points because the curvature of the water interfaces is greater. A experimental study of sliding behaviour by Emerson and Rempel (2007) pointed to particle size and concentration controls on sliding behaviour. They distinguish a "sandy" regime in which there is relatively high resistance to sliding associated with higher debris concentration and larger particle sizes. By contrast, when debris concentrations are lower and particle sizes are smaller there is an abrupt transition into a "slippery" regime in which shear resistance is no longer dependent on normal load. The physical characteristics of the debris-rich basal ice in Taylor Glacier together with the high solute concentrations (Table 2) and presence of fine-grained particles (Figure 8) seems to be compatible with larger volumes of premelted liquid and lower friction. Further evidence for the presence of premelted liquid in the basal ice of Taylor Glacier was provided by Samyn et al. (2005a) who suggested that subtle changes in the gas composition were typical of phase changes involving minute quantities of water and crystallographic evidence of lattice loosening indicate small-scale strain variations that are compatible with slight changes in water content.

4.3 Origin and evolution of the basal zone

The basal ice facies observed in tunnels in Taylor Glacier bear some striking similarities to the model of basal ice formation under freezing conditions proposed by Christoffersen et al. (2006). These authors developed a numerical model for basal ice formation based on the ratio of the supply of subglacial water to the freezing rate in which the following types of ice are produced depending on the subglacial hydrology: clear ice is produced when water is freely available; laminated ice if the supply of water is constrained; massive ice if the water supply is further constrained; and a solid facies if meltwater is depleted and there is rapid freezing. The massive subfacies observed beneath Taylor Glacier is structurally very similar to the modelled massive facies because it consists of finely stacked laminae that appear to be massive from visual observation (Figure 4 c and d). A regelation origin for the massive and laminated subfacies is consistent with many lines of evidence for the presence of liquid water beneath Taylor Glacier (Hubbard et al., 2004; Mikucki et al., 2015; Badgeley et al., 2017; Lyons et al., 2019) and with cooling of the base of the glacier as it thins toward the margin.

A significant difference with these regelation model proposed by Christoffersen et al. (2006) is that the Taylor Glacier basal ice layer consists of the debris bearing ice interbedded with clean bubbly englacial ice. This interbedding together with abundant evidence of sinistral rotation described above, the presence of recumbent folds and the development of parasitic folds suggests that tectonic processes play a role in basal ice formation. The occurrence of tight recumbent folds in the laminated subfacies (Figure 6c) and the interbedded nature of the laminated subfacies with the englacial facies suggests that debris bearing-ice is being mixed with adjacent relatively clean ice. Such mixing is to be expected at structural boundaries where there are rheological contrasts, an association that is well known to lead to flow perturbations in shear zones (Ramsay & Huber, 1987; Passchier & Simpson, 1986). These perturbations first lead to basal zone thickening, then to shortening and stretching. Because of the pervasive simple shear in the basal zone the folds are likely to be rapidly attenuated into the planar structures that characterize the bulk of ice in the basal zone. From the observed deformation structures together with the patterns of deformation we conclude that there is tectonic evolution of the basal ice along the flow path toward the glacier margin. We suggest that the laminated subfacies is at least partly a tectonic facies that is derived from mechanical deformation at the upper and lower boundaries of the massive subfacies. This tectonic origin is further supported by gas chromatography (Samyn et al., 2005a) and water co-isotopic measurements (Souchez et al., 2004), both conducted at the cm-scale within the basal ice zone, showing that the clean and debris-bearing ice layers from the laminated subfacies present a ‘meteoric’ signature, thereby precluding their origin as resulting from macro-scale regelation process.

The tunnel walls show that the basal ice layers rise toward the ice margin and that at some locations there is an abrupt termination of the basal debris layers before the ice cliff (Figure 2). This termination appears to the product of partial overriding and entrainment of the ice apron that forms at the foot of the terminal cliff in places. The process of apron entrainment has been described by Shaw (1977) and Fitzsimons et al. (2008).

4.4 Implications for glacier behaviour

554 Displacements measured in the tunnel show that the basal zone contributes about 1.5 m
555 of motion per year which is about 60% of the 2.5 $m.a^{-1}$ surface velocity at the ice edge. The same
556 value of basal motion was observed in "ice-laden drift" with a temperature of -4°C in Urumqui
557 No 1 Glacier (Echelmeyer & Zhongxiang, 1987). Similar results have also been reported from
558 Russell Glacier, a polythermal outlet glacier from Greenland where 16% of the motion was
559 attributed to deformation of basal ice (Waller & Hart, 1999). At Taylor Glacier a previous study
560 (Petit et al., 2014) used a two-layer flow model to predict the basal properties of Taylor Glacier
561 and concluded that deformation of the basal ice layer accounted for 85 to 98% of glacier motion,
562 that the basal ice layer was likely 10-15 m thick, and that the basal ice was 20-40 times softer
563 that clean englacial ice. While the measurements made in the tunnel are broadly consistent with
564 the argument that the basal ice layer plays a significant role in the behaviour of Taylor Glacier,
565 the basal ice layer that we have characterized is thinner, does not account for such a large
566 proportion of surface motion and is only 2 times softer than the values concluded by Pettit et al.
567 (2014).

568 One of the issues in examining the behaviour of ice and debris at the base of glaciers is
569 that there is a continuum between debris-rich basal ice and ice-rich debris that might form the
570 bed of a glacier. What one researcher might describe as basal ice another might describe as ice-
571 rich sediment or frozen till. This problem is exacerbated when observations are made using bore
572 holes because of uncertainties concerning the location of the glacier bed and because the holes
573 cannot penetrate coarse sediment, unless local conditions allow diamond drilling equipment to be
574 deployed (e.g. Truffer et al., 2000). For example, work by Echelmeyer and Zhongxiang (1987) is
575 widely cited as evidence for subglacial deformation in subfreezing conditions. However, their
576 description of the contact between the glacier bed and the substrate as a junction between clear
577 glacier ice with a low debris content and the bed samples of which contain 21-39% debris. In
578 Taylor Glacier such a boundary occurs between the englacial ice and the laminated subfacies,
579 which is contained entirely within the debris-bearing basal ice. Although the tunnel-based
580 observations at Taylor Glacier leave little doubt that the measurements have been made within
581 the basal ice layer (Figure 4), it is clear that the displacement profile measured through the basal
582 zone resembles that of a subglacial sediment deformation profile (e.g. Boulton & Hindmarsh,
583 1987; Boulton, 2006) because the strain is heterogenous and the velocity profiles are stepped
584 because of the presence of offsets which appear to be due to sliding. The observations made in
585 the tunnels support the view that the base of glaciers should be defined as a zone, not a single
586 zero-velocity boundary at a simple ice-substrate interface (Waller, 2001, Fitzsimons, 2006; Pettit
587 et al., 2014).

588 4.5. Implications for glacial geology

589 Our measurements show that the basal zone has an emergence velocity of around 1.5 m a^{-1}.,
590 i.e. the velocity at which it arrives at the ice edge. The average debris concentration through
591 massive subfacies is 26% by volume for a 1.2 m-thick layer and for the laminated subfacies is
592 12% vol. for 1.6 m-thick layer which together yields 0.5 m^3. a^{-1} of debris per 1 m of ice margin
593 per year. These estimates are half the estimate made by Pettit et al. (2014). The difference in our
594 calculations are that the emergence velocity is lower, the thickness of the basal layers
595 substantially smaller (4.5 m vs. 10 m) although the measured debris concentrations in the basal
596 ice are much greater than those suggested by Pettit et al. (2014). The volume of debris that is
597 discharged to the ice margin is not consistent with the modest accumulations of material that has

accumulated along the ice edge and absence of moraines (Figure 1). There are no substantial accumulations of material at the ice margin because fluvial processes rapidly remove most of the debris that that is discharged from the ice cliff. A steep ephemeral marginal meltwater stream, Santa Fe Creek, is pinned against the ice margin by the adverse slope adjacent to the ice edge (Figure 1). Consequently all the fine-grained sediment excavated from the basal zone was removed and transported into Lake Bonney within one year of the excavations. A boulder and cobble lag was all that remained. An exception to this process is the small ice cored moraine that rests on the delta of Santa Fe Creek adjacent to Blood Falls at the glacier terminus. Basal ice is preserved in the core of this moraine, and ablation of the ice has produced a silty till with numerous facetted and striated clasts. This material is indistinguishable from the basal ice observed in the tunnels.

A combination of high debris concentrations in the debris-bearing ice and the high shear experienced within the ice has produced facetted and abraded clasts and a high proportion of silt-sized particles in particle size distributions. These characteristics are similar to the sedimentary signature of temperate glacial environments which are dominated by high rates of abrasion and contrast strongly with the sedimentary signature of cold-based glaciers which are dominated by sandy gravel, glacitectonically deformed permafrost and aeolian deposits (Hambrey & Fitzsimons, 2010; Hambrey & Glasser, 2012; Fitzsimons & Howarth, 2020). These observations highlight the complexity of basal ice processes at the margin of Taylor Glacier and that simple sedimentological criteria may not always be a sound basis for reconstructing glaciers with different thermal regimes.

5 Conclusions

The basal zone of Taylor Glacier is characterized by a complex strain distribution that results from heterogeneous deformation within the basal zone. The strongest materials and lowest rates of deformation occur in ice layers with low debris concentrations and the weakest materials and highest rates of deformation occur in layers of ice with the highest debris concentrations and high solute loads. Ice with a laminated appearance has an intermediate strength.

Deformation of the whole basal zone accounts for 60% of glacier motion at this ice marginal location. Velocity profiles determined using plumblines suggest that either the ice is sliding at structural interfaces or that high rates of shear are localized to in narrow (<100 mm) zones accounting for 14% of glacier motion. Short term measurement of displacements using engineers dial gauges together with the development of cavities and slickenslides in the ice support the interpretation of sliding of up to 167 $mm.a^{-1}$ or very localized interfacial flow despite the low basal temperature (-18°C). These observations are consistent with studies of ice crystallography which show that evidence of pervasive shearing and strain localization at sedimentological and structural interfaces (Samyn et al., 2008).

Heterogeneous deformation results in flow perturbations which cause folding which drives mixing within the basal zone which results in blending of debris-bearing and clean ice facies. Mixing of adjacent ice facies results in tectonic evolution of the basal ice along the flow line together with basal zone thickening toward the margin of the glacier. Deformation

measurements together with observations of folding and shearing suggest that at least part of the laminated subfacies has been produced by mechanical deformation within the basal zone.

High rates of strain combined with high debris concentrations in the debris-bearing ice produce a high abrasion environment which is consistent with abundant heavily facetted and striated clasts and a strong silt mode in particle size distributions. The combination of the sedimentary signature of the abraded and facetted particles, the production of high volumes of silt-sized particles and the relatively high sediment flux of the basal zone are characteristics normally associated with temperate glaciers. However, the structural and geochemical signature of the basal profile reflects the cold nature of the marginal ice.

Finally, our observation of the structure, composition and deformation of basal ice in Taylor Glacier support the view that glacier beds are zones in which deformation is spatially and temporally variable. Our observations and measurements how that the glacier bed is not as a single zero-velocity boundary further suggest that glacier flow models need to incorporate rheologically distinct layers to capture spatially variable behaviour of debris bearing basal ice (e.g. Petit et al., 2014).

Acknowledgments

This work was supported by the Marsden Fund, Royal Society of NZ grant "Direct observations of basal ice and substrate deformation at subfreezing temperatures". The University of Otago and the Belgian Antarctic Programme also supported the work and logistical support was provided by Antarctica New Zealand to Event K064. We thank Dr. Kevin McManus, formerly of the Department of Civil Engineering, University of Canterbury for providing the direct shear device and modifying it for use in the tunnel. We are grateful for field assistance provided by Marcus Vandergoes, Mike Hambrey, Paul Sirota, Tracey Morgan, Vaughn Filmer and Katrin Rohl. Chris Garden designed and drew the diagrams.

Open Research

The data collected during the field study together with video clips of the excavation and additional photographs of the tunnels and basal ice are available at https://doi.org/10.5281/zenodo.8232003 (Fitzsimons, 2023).

References

Alley, R. B., Cuffey, K. M., Evenson, E. B., Strasser, J. C., Lawson, D. E., & Larson, G. J. (1997). How glaciers entrain and transport basal sediment: Physical constraints. *Quaternary Science Reviews,* 16(9), 1017–1038. https://doi.org/10.1016/s0277-3791(97)00034-6

Alley, R. B., Cuffey, K. M., & Zoet, L. K. (2019). Glacial erosion: status and outlook. *Annals of Glaciology*, 60(80), 1–13. https://doi.org/10.1017/aog.2019.38

Astakhov, V. I., Kaplyanskaya, F. A., & Tarnogradsky, V. D. (1996). Pleistocene permafrost of West Siberia as a deformable glacier bed. *Permafrost and Periglacial Processes*, 7(2),

165–191. https://doi.org/10.1002/(sici)1099-1530(199604)7:2<165::aid-ppp218>3.0.co;2-s

Badgeley, J. A., Pettit, E. C., Carr, C. G., Tulaczyk, S., Mikucki, J. A., & Lyons, W. B. (2017). An englacial hydrologic system of brine within a cold glacier: Blood Falls, McMurdo Dry Valleys, Antarctica. *Journal of Glaciology*, 63(239), 387–400. https://doi.org/10.1017/jog.2017.16

Boulton, G. S. (2006). Glaciers and their Coupling with Hydraulic and Sedimentary Processes. *Glacier Science and Environmental Change*, 2–22. https://doi.org/10.1002/9780470750636.ch2

Boulton, G. S., & Hindmarsh, R. C. A. (1987). Sediment deformation beneath glaciers: Rheology and geological consequences. *Journal of Geophysical Research*, 92(B9), 9059. https://doi.org/10.1029/jb092ib09p09059

Christoffersen, P., Tulaczyk, S., Carsey, F. D., & Behar, A. E. (2006). A quantitative framework for interpretation of basal ice facies formed by ice accretion over subglacial sediment. *Journal of Geophysical Research*, 111(F1). https://doi.org/10.1029/2005jf000363

Clarke, G. K. C. (2005). Subglacial Processes. *Annual Review of Earth and Planetary Sciences*, 33(1), 247–276. https://doi.org/10.1146/annurev.earth.33.092203.122621

Cohen, D. (2000), Rheology of ice at the bed of Engabreen, Norway, J. Glaciol., 46(155), 611–621. https://doi:10.3189/172756500781832620

Cuffey, K. M., Conway, H., Hallet, B., Gades, A. M., & Raymond, C. F. (1999). Interfacial water in polar glaciers and glacier sliding at −17°C. *Geophysical Research Letters*, 26(6), 751–754. https://doi.org/10.1029/1999gl900096

Cuffey, K. M., Conway, H., Gades, A., Hallet, B., Raymond, C. F., & Whitlow, S. (2000). Deformation properties of subfreezing glacier ice: Role of crystal size, chemical impurities, and rock particles inferred from in situ measurements. *Journal of Geophysical Research: Solid Earth*, 105(B12), 27895–27915. https://doi.org/10.1029/2000jb900271

Dash, J. G., Fu, H., & Wettlaufer, J. S. (1995). The premelting of ice and its environmental consequences. *Reports on Progress in Physics*, 58(1), 115–167. https://doi.org/10.1088/0034-4885/58/1/003

Dash, J. G., Rempel, A. W., & Wettlaufer, J. S. (2006). The physics of premelted ice and its geophysical consequences. *Reviews of Modern Physics*, 78(3), 695–741. https://doi.org/10.1103/revmodphys.78.695

Echelmeyer, K., & Zhongxiang, W. (1987). Direct Observation of Basal Sliding and Deformation of Basal Drift at Sub-Freezing Temperatures. *Journal of Glaciology*, 33(113), 83–98. https://doi.org/10.3189/s0022143000005396

Emerson, L. F., & Rempel, A. W. (2007). Thresholds in the sliding resistance of simulated basal ice. *The Cryosphere*, 1(1), 11–19. https://doi.org/10.5194/tc-1-11-2007

Fitzsimons, S. (2006). Mechanical Behaviour and Structure of the Debris-Rich Basal Ice Layer. In *Glacier Science and Environmental Change* (pp. 329–335). Blackwell. https://doi.org/10.1002/9780470750636.ch65

Sean Fitzsimons. (2023). Taylor Glacier Tunnel: Measurements of the composition, deformation and strength of basal ice made in a tunnel in Taylor Glacier, Antarctica [Data set]. Zenodo. https://doi.org/10.5281/zenodo.8232003

Fitzsimons, S., & Howarth, J. (2020). Development of push moraines in deeply frozen sediment adjacent to a cold-based glacier in the McMurdo Dry Valleys, Antarctica. *Earth Surface Processes and Landforms*, 45(3), 622–637. https://doi.org/10.1002/esp.4759

Fitzsismons, S. J., McManus, K. J., & Lorrain, R. D. (1999). Structure and strength of basal ice and substrate of a dry-based glacier: evidence for substrate deformation at sub-freezing temperatures. *Annals of Glaciology*, 28, 236–240. https://doi.org/10.3189/172756499781821878

Fitzsimons, S. J., Lorrain, R. D., & Vandergoes, M. J. (2000). Behaviour of subglacial sediment and basal ice in a cold glacier. *Geological Society, London, Special Publications*, 176(1), 181–190. https://doi.org/10.1144/gsl.sp.2000.176.01.14

Fitzsimons, S. J., McManus, K. J., Sirota, P., & Lorrain, R. D. (2001). Direct shear tests of materials from a cold glacier: implications for landform development. *Quaternary International*, 86(1), 129–137. https://doi.org/10.1016/s1040-6182(01)00055-6

752 Fitzsimons, S., Webb, N., Mager, S., MacDonell, S., Lorrain, R., & Samyn, D. (2008).
753 Mechanisms of basal ice formation in polar glaciers: An evaluation of the apron
754 entrainment model. *Journal of Geophysical Research*, 113(F2).
755 https://doi.org/10.1029/2006jf000698

756

757 Fitzsimons, S., Sharp, M., & Lorrain, R. (2023). Subglacial deformation of permafrost beneath
758 Wright Lower Glacier, Antarctica as revealed by direct observations and measurements
759 from a subglacial tunnel. *Geomorphology*, 440, 108886.
760 https://doi.org/10.1016/j.geomorph.2023.108886

761

762 Foley, N., Tulaczyk, S., Auken, E., Schamper, C., Dugan, H., Mikucki, J., Virginia, R., & Doran,
763 P. (2016). Helicopter-borne transient electromagnetics in high-latitude environments: An
764 application in the McMurdo Dry Valleys, Antarctica. *Geophysics*, 81(1), WA87–WA99.
765 https://doi.org/10.1190/geo2015-0186.1

766

767 Fowler, A. C. (1986). Sub-Temperate Basal Sliding. *Journal of Glaciology*, 32(110), 3–5.
768 https://doi.org/10.3189/s0022143000006808

769

770 Gilpin, R. R. (1979). A model of the "liquid-like" layer between ice and a substrate with
771 applications to wire regelation and particle migration. *Journal of Colloid and Interface*
772 *Science*, 68(2), 235–251. https://doi.org/10.1016/0021-9797(79)90277-7

773

774 Goughnour, R. R., & Andersland, O. B. (1968). Mechanical Properties of a Sand-Ice System.
775 Journal of the Soil Mechanics and Foundations Division, 94(4), 923–950.
776 https://doi.org/10.1061/jsfeaq.0001179

777

778 Hambrey, M. J., Milnes, A. G., & Siegenthaler, H. (1980). Dynamics and Structure of
779 Griesgletscher, Switzerland. *Journal of Glaciology*, 25(92), 215–228.
780 https://doi.org/10.3189/s0022143000010455

781

782 Hambrey, M. J., & Müller, F. (1978). Structures and Ice Deformation in the White Glacier, Axel
783 Heiberg Island, Northwest Territories, Canada. *Journal of Glaciology*, 20(82), 41–66.
784 https://doi.org/10.3189/s0022143000021213

785

786 Holdsworth, G. (1974). Meserve Glacier Wright Valley, Antarctica: Part I. Basal
787 Processes.Institute of Polar Studies Report No. 37, Ohio State University, Columbus,
788 Ohio.

789

Hubbard, B. (2006). On the Relationships Between Field Data and Numerical Models of Ice-Mass Motion. *Glacier Science and Environmental Change*, 338–345. https://doi.org/10.1002/9780470750636.ch67

Hubbard, B., Cook, S., & Coulson, H. (2009). Basal ice facies: a review and unifying approach. *Quaternary Science Reviews*, 28(19–20), 1956–1969. https://doi.org/10.1016/j.quascirev.2009.03.005

Hubbard, A., Lawson, W., Anderson, B., Hubbard, B., & Blatter, H. (2004). Evidence for subglacial ponding across Taylor Glacier, Dry Valleys, Antarctica. *Annals of Glaciology*, 39, 79–84. https://doi.org/10.3189/172756404781813970

Hubbard, B., & Sharp, M. (1989). Basal ice formation and deformation: a review. *Progress in Physical Geography: Earth and Environment,* 13(4), 529–558. https://doi.org/10.1177/030913338901300403

Hubbard, B., & Sharp, M. (1993). Weertman regelation, multiple refreezing events and the isotopic evolution of the basal ice layer. *Journal of Glaciology*, 39(132), 275–291. https://doi.org/10.3189/s002214300001594x

Iverson, N. R. (2010). Shear resistance and continuity of subglacial till: hydrology rules. *Journal of Glaciology*, 56(200), 1104–1114. https://doi.org/10.3189/002214311796406220

Jacka, T. H., Shavawn Donoghue, Li, J., William F. Budd, & Anderson, R. M. (2003). Laboratory studies of the flow rates of debris-laden ice. Annals of Glaciology, 37, 108–112. https://doi.org/10.3189/172756403781815537

Lawson, W. (1996). The relative strengths of debris-laden basal ice and clean glacier ice: some evidence from Taylor Glacier, Antarctica. *Annals of Glaciology*, 23, 270–276. https://doi.org/10.3189/s0260305500013537

Lyons, W. B., Mikucki, J. A., German, L. A., Welch, K. A., Welch, S. A., Gardner, C. B., Tulaczyk, S. M., Pettit, E. C., Kowalski, J., & Dachwald, B. (2019). The Geochemistry of Englacial Brine From Taylor Glacier, Antarctica. *Journal of Geophysical Research: Biogeosciences*, 124(3), 633–648. Portico. https://doi.org/10.1029/2018jg004411

Montross, S., Skidmore, M., Christner, B., Samyn, D., Tison, J.-L., Lorrain, R., Doyle, S., & Fitzsimons, S. (2013). Debris-Rich Basal Ice as a Microbial Habitat, Taylor Glacier,

828 Antarctica. *Geomicrobiology Journal*, 31(1), 76–81.
829 https://doi.org/10.1080/01490451.2013.811316

830

831 Moore, P. L. (2014). Deformation of debris-ice mixtures. *Reviews of Geophysics*, *52*(3), 435-
832 467.

833

834 Mikucki, J. A., Auken, E., Tulaczyk, S., Virginia, R. A., Schamper, C., Sørensen, K. I., Doran, P.
835 T., Dugan, H., & Foley, N. (2015). Deep groundwater and potential subsurface habitats
836 beneath an Antarctic dry valley. Nature Communications, 6(1).
837 https://doi.org/10.1038/ncomms7831

838

839 Nickling, W. G., & Bennett, L. (1984). The Shear Strength Characteristics of Frozen Coarse
840 Granular Debris. Journal of Glaciology, 30(106), 348–357.
841 https://doi.org/10.1017/s0022143000006201

842

843 Passchier, C. W., & Simpson, C. (1986). Porphyroclast systems as kinematic indicators. *Journal*
844 *of Structural Geology*, 8(8), 831–843. https://doi.org/10.1016/0191-8141(86)90029-5

845

846 Pettit, E. C., Whorton, E. N., Waddington, E. D., & Sletten, R. S. (2014). Influence of debris-rich
847 basal ice on flow of a polar glacier. *Journal of Glaciology*, 60(223), 989–1006.
848 https://doi.org/10.3189/2014jog13j161

849

850 Powers, M. C. (1953). A New Roundness Scale for Sedimentary Particles. *SEPM Journal of*
851 *Sedimentary Research*, Vol. 23. https://doi.org/10.1306/d4269567-2b26-11d7-
852 8648000102c1865d

853

854 Ramsay, J. G., (1967). *Folding and Fracturing of Rocks*. McGraw Hill, New York. 568 pp.

855

856 Ramsay, J.G. & Huber, M. I. (1987). The techniques of modern structural geology. Folds and
857 Fractures, Vol. 2. Academic Press.

858

859 Rabus, B. T., & Echelmeyer, K. A. (1997). The flow of a polythermal glacier: McCall Glacier,
860 Alaska, U.S.A. Journal of Glaciology, 43(145), 522–536.
861 https://doi.org/10.3189/s0022143000035139

862

863 Rempel, A. W., Meyer, C. R., & Riverman, K. L. (2021). Melting temperature changes during
864 slip across subglacial cavities drive basal mass exchange. *Journal of Glaciology*, 68(267),
865 197–203. https://doi.org/10.1017/jog.2021.107

Robinson, P. H. (1984). Ice dynamics and thermal regime of Taylor Glacier, South Victoria Land, Antarctica. *Journal of Glaciology*, 30(105), 153– 160. https://doi.org/10.1017/S0022143000005888

Samyn, D., Fitzsimons, S. J., & Lorrain, R. D. (2005a). Strain-induced phase changes within cold basal ice from Taylor Glacier, Antarctica, indicated by textural and gas analyses. *Journal of Glaciology*, 51(175), 611–619. https://doi.org/10.3189/172756505781829098

Samyn, D., Fitzsimons, S. J., & Lorrain, R. D. (2009). Rotating micro-structures in Antarctic cold basal ice: implications for glacier flow and its interpretation. *International Journal of Earth Sciences*, 99(8), 1849–1857. https://doi.org/10.1007/s00531-009-0478-5

Samyn, D., Svensson, A., & Fitzsimons, S. J. (2008). Dynamic implications of discontinuous recrystallization in cold basal ice: Taylor Glacier, Antarctica. *Journal of Geophysical Research*, 113(F3). https://doi.org/10.1029/2006jf000600

Samyn D., Svensson A., Fitzsimons S.J., & Lorrain R. (2005b). Ice crystalproperties of amber ice and strain enhancement at the base of cold Antarctic glaciers. *Annals of Glaciology* 40:185–190. https://doi.org/10.3189/172756405781813618

Sharp, M., Lawson, W., & Anderson, R. S. (1988). Tectonic processes in a surge-type glacier. *Journal of Structural Geology*, 10(5), 499–515. https://doi.org/10.1016/0191-8141(88)90037-5

Shaw, J. (1977). Till body morphology and structure related to glacier flow. *Boreas*, 6(2), 189–201. https://doi.org/10.1111/j.1502-3885.1977.tb00348

Shreve, R. L. (1984). Glacier Sliding at Subfreezing Temperatures. *Journal of Glaciology*, 30(106), 341–347. https://doi.org/10.3189/s0022143000006195

Simpson, C., & De Paor, D. G. (1993). Strain and kinematic analysis in general shear zones. *Journal of Structural Geology*, 15(1), 1–20. https://doi.org/10.1016/0191-8141(93)90075-l

Souchez, R., Samyn, D., Lorrain, R., Pattyn, F. & Fitzsimons, S. (2004). An isotopic model for basal freeze-on associated with subglacial upward flow of pore water. *Geophys. Res. Lett.* 31:L02401. https://doi.org/10.1029/2003GL018861

Thompson, A. C., Iverson, N. R., & Zoet, L. K. (2020). Controls on Subglacial Rock Friction: Experiments With Debris in Temperate Ice. Journal of Geophysical Research: Earth Surface, 125(10). https://doi.org/10.1029/2020jf005718

Truffer, M., Harrison, W. D., & Echelmeyer, K. A. (2000). Glacier motion dominated by processes deep in underlying till. *Journal of Glaciology*, 46(153), 213–221. https://doi.org/10.3189/172756500781832909

Waller, R. I. (2001). The influence of basal processes on the dynamic behaviour of cold-based glaciers. *Quaternary International*, 86(1), 117–128. https://doi.org/10.1016/s1040-6182(01)00054-4

Waller, R.I. & Hart, J.K.. (1999). Mechanisms and patterns of motion associated with the basal zone of the Russell Glacier, south-west Greenland. *Journal of Glacial Geology and Geomorphology*, 21, 1–20.

Waller, R. I., Murton, J. B., & Kristensen, L. (2012). Glacier–permafrost interactions: Processes, products and glaciological implications. Sedimentary Geology, 255–256, 1–28. https://doi.org/10.1016/j.sedgeo.2012.02.005

Warbritton, M. J., Iverson, N. R., Lagroix, F., and Schomacker, A. (2020). Strain patterns in glacitectonically thrusted sediments and conditions during thrusting. *Journal of Structural Geology*, 137, 104064. https://doi.org/10.1016/j.jsg.2020.104064

Wettlaufer, J. S. (1999). Impurity Effects in the Premelting of Ice. *Physical Review Letters*, 82(12), 2516–2519. https://doi.org/10.1103/physrevlett.82.2516

Wettlaufer, J. S., Worster, M. G., Wilen, L. A., & Dash, J. G. (1996). A Theory of Premelting Dynamics for all Power Law Forces. *Physical Review Letters*, 76(19), 3602–3605. https://doi.org/10.1103/physrevlett.76.3602